Clusters, Radicals, and Ions; Environmental Chemistry

# Stereoselectivity in Atmospheric Autoxidation

Kristian H. Møller, Eric Joseph Praske, Lu Xu, John D. Crounse, Paul O. Wennberg, and Henrik Grum Kjaergaard

*J. Phys. Chem. Lett.*, **Just Accepted Manuscript** • DOI: 10.1021/acs.jpclett.9b01972 • Publication Date (Web): 23 Sep 2019

# Stereoselectivity in Atmospheric Autoxidation

Kristian H. Møller,[†] Eric Praske,[‡] Lu Xu,[¶] John D. Crounse,[¶] Paul O. Wennberg,[*,¶,§] and Henrik G. Kjaergaard[*,†]

†*Department of Chemistry, University of Copenhagen, DK-2100 Copenhagen Ø, Denmark*

‡*Division of Chemistry and Chemical Engineering, California Institute of Technology, Pasadena, California 91125, United States*

¶*Division of Geological and Planetary Sciences, California Institute of Technology, Pasadena, California 91125, United States*

§*Division of Engineering and Applied Science, California Institute of Technology, Pasadena, California 91125, United States*

E-mail: wennberg@caltech.edu; hgk@chem.ku.dk

**Abstract**

We show that the diastereomers of hydroxy peroxy radicals formed from OH and $O_2$-addition to C2 and C3, respectively, of crotonaldehyde ($CH_3CHCHCHO$), undergo gas-phase unimolecular aldehydic hydrogen shift (H-shift) chemistry with rate coefficients that differ by an order of magnitude. The stereospecificity observed here for crotonaldehyde is general and will lead to a significant diastereomeric-specific chemistry in the atmosphere. This enhancement of specific stereoisomers by stereoselective gas-phase reactions could have widespread implications given the ubiquity of chirality in nature. The H-shift rate coefficients calculated using multi-conformer transition state theory (MC-TST) agree with those determined experimentally using stereoisomer-specific gas-chromatography chemical ionization mass spectroscopy (GC-CIMS) measurements.

# Graphical TOC Entry

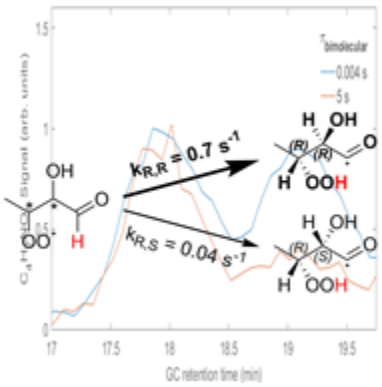


Most of the molecules central to life, including DNA, amino acids and sugars, are chiral.[1,2] Typically, one chiral form of molecules exist in nature; sugars, for example, are found almost exclusively as the D-form, while amino acids occur naturally as the L-form, and the origin of this homochirality is a great mystery.[1–3]

Many biogenically- and anthropogenically-produced compounds emitted into the atmosphere are chiral.[4,5] Several studies have found that the enantiomeric composition of VOCs (including the important monoterpenes) vary with biome, plant type, season, time of day and stress factors.[6–10] For instance, it has been observed that, in tropical regions, (-)-$\alpha$-pinene dominates the emissions, while (+)-$\alpha$-pinene has been found to dominate in a boreal forest.[6]

Both experiments and field measurements have shown transfer of precursor chirality into formed seconday organic aerosol (SOA).[11–14] Studies of polymers suggest that stereochemistry can affect the physical properties of the aerosol, such as hydrophilicity, phase behavior, intramolecular hydrogen bonding and molecular macrostructure.[15–19] This in turn may affect the aerosol rate of growth, their ability to act as a cloud condensation nuclei (CCN) and radiative properties, thus affecting their influence on Earth's climate.[20–22]

Enhancement of specific stereoisomers can arise from differences in rate coefficients of dif-

ferent stereoisomers, i.e. stereoselectivity. A decade ago, surface stereochemical effects were observed for heterogeneous ozonolysis (about a factor of two difference between different diastereomers) and were suggested as a potential route to chiral excess in prebiotic chemistry.[23] It has also been speculated, that oligomerization of epoxides formed in isoprene oxidation at aerosol surfaces could similarly be stereoselective.[19] Stereoselectivity in gas-phase reactions has so far been elusive.

We investigate the diastereomeric selectivity in unimolecular gas-phase peroxy radical hydrogen shift (H-shift) reactions. These H-shift reactions have been linked to the formation of highly oxidized molecules that are important for the growth of SOA in the atmosphere.[24–29] Recent global modeling suggests that at least 30 % of all isoprene molecules emitted to the atmosphere undergo a minimum of one H-shift during its oxidation cascade highlighting the importance of these reaction pathways.[30] Peroxy radical H-shift reactions are unimolecular reactions in which a peroxy radical abstracts a hydrogen atom from another location in the same molecule. Organic peroxy radicals in atmospheric oxidation are typically formed from $O_2$-addition to a near-planar alkyl radical center.[31,32] If the three substituents at the alkyl radical are different, $O_2$-addition will form a new chiral center. Generally, this $O_2$-addition is expected to form comparable amounts of the two stereoisomers leading to a racemic mixture. For compounds with an existing chiral center, this leads to a set of four stereoisomers, as shown in Figure 1. The enantiomers, which are inverted at both chiral centers [e.g. *(R,R)* and *(S,S)* labeled *(R*,R*)* here], are mirror images of each other and thus have the same physio-chemical properties including unimolecular reaction rate coefficients and bimolecular rate coefficients with achiral reaction partners.[33] The diastereomers on the other hand, differ at only one of the stereocenters and have different properties.[33] We refer to the diastereomers with the same configuration at both chiral centers as *(R*,R*)* and those with different configuration as *(R*,S*)*.

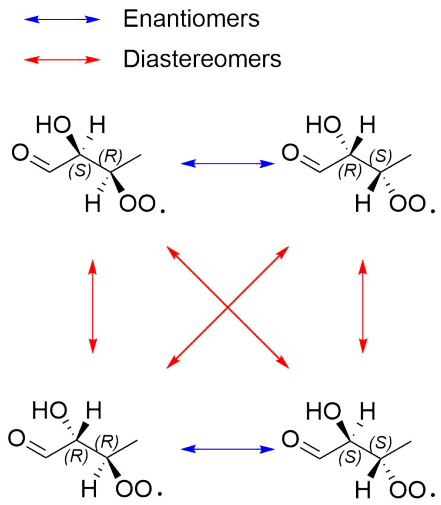


Figure 1: Relation between the four stereoisomers comprising one of the structural isomers of crotonaldehyde hydroxy peroxy radical, 2-OH,3-OO-CRALD.

We are at a point in time where these peroxy radical H-shifts are being implemented into global atmospheric chemistry models.[34,35] It is therefore imperative that the stereoselectivity, which has been suggested by recent theoretical studies,[24,30,36–39] is evaluated experimentally. The importance of stereoselectivity in the atmosphere is two fold. Firstly, the rate coefficients can differ significantly between the different diastereomers and thus both need to be considered.[30] Secondly, it affects the stereochemistry of the formed products and may lead to significant stereoselective enhancement.

Here, we demonstrate stereoselectivity in a pair of diastereomers formed in the hydroxyl radical initiated oxidation of an alkene aldehyde, crotonaldehyde (2-butenal, CRALD), see Figures 1 and 2. Using stereoisomer-specific gas-chromatography chemical ionization mass spectrometry (GC-CIMS) measurements of the hydroxy nitrates (HN) formed by reaction of the peroxy radicals with NO, we probe the competition between bimolecular and unimolecular chemistry to quantify the rate coefficients of the peroxy H-shifts, using an approach similar to that employed previously for other systems.[40–42] As such, we provide the first experimental demonstration of stereoselectivity in peroxy radical H-shifts, which is now recognized as a major atmospheric route to formation of secondary organic aerosol.[24–27,29] The

experimentally determined rate coefficients are compared to those obtained using multi-conformer transition state theory (MC-TST).[36,43]

Crotonaldehyde reacts with hydroxyl (OH) radicals with a rate coefficient of about $3.4\times10^{-11}$ $cm^3$ $molecule^{-1}$ $s^{-1}$ at room temperature.[44–46] The reaction is expected to progress by either OH-addition to the double bond or abstraction of the aldehydic H-atom (see Figure 2).[46,47] Experimental studies and structure-activity relationships (SARs) suggest that the two pathways are likely comparable.[44,46–48] The addition products are the primary focus of this study. The hydroxy peroxy radicals formed by OH and subsequent $O_2$-addition retain the labile aldehydic hydrogen and are thus expected to undergo fast aldehydic H-shifts.[30,49]

As shown in Figure 2, OH can add to crotonaldehyde at either the 2 or 3-position yielding two different alkyl radical structural isomers. The subsequent reaction step is addition of molecular oxygen to yield the hydroxy peroxy radicals 2-OH,3-OO-CRALD and 3-OH,2-OO-CRALD. As shown in Figure 2, both structural isomers can undergo unimolecular H-shifts or react bimolecularly with NO to form hydroxy nitrates (HN).

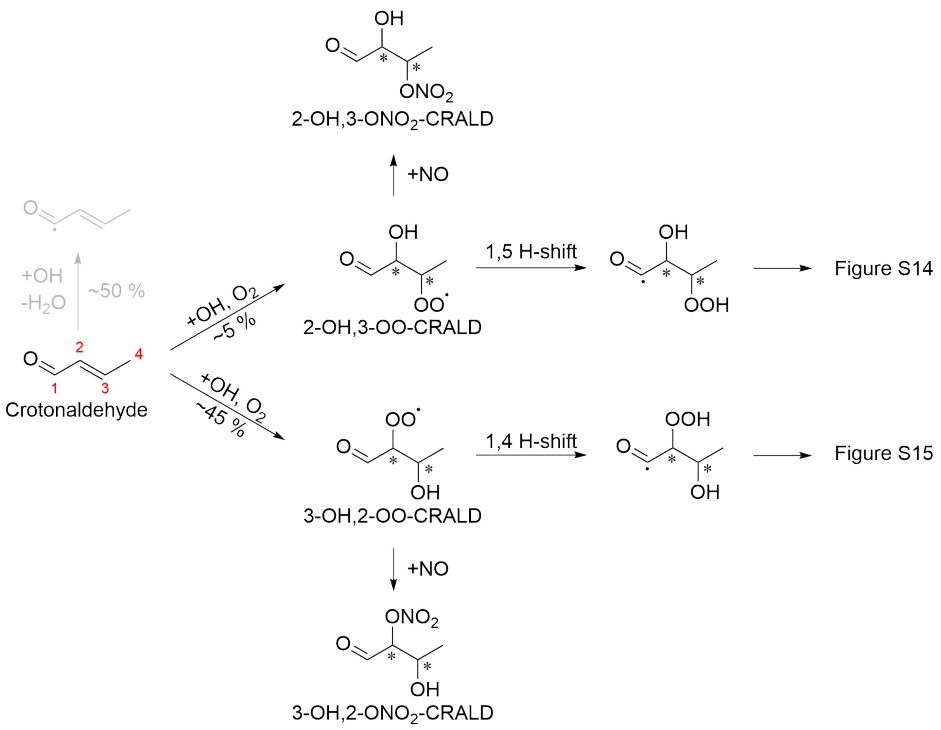


Figure 2: Mechanism for formation of the crotonaldehyde hydroxy nitrates and competing unimolecular aldehydic H-shifts. The two chiral centers are indicated by asterisks. The H-abstraction pathway shown in grey is not important for the kinetic study here but included for completeness. The branching between addition and abstraction is based on literature,[44,46–48] while the branching between the two addition pathways is estimated experimentally here.

In the post-oxidation gas chromatograms (Figure 3) four peaks are observed at m/z 234 corresponding to the adduct of the crotonaldehyde hydroxy nitrates with $CF_3O^-$. High mass resolution data ($(m/z)/\Delta(m/z) \sim 3500$) confirm this chemical composition. As our experimental setup does not distinguish enantiomers, this is what we would expect from the mechanism in Figure 2 with two diastereomers [*(R*,R*)* and *(R*,S*)*] for each structural isomer. Addition of OH to the 3-position yields a resonance stabilized alkyl radical (confirmed theoretically to be significantly more stable, see Table S13) and this is expected to be the major pathway. Thus, we assign the two large (later-eluting) peaks in Figure 3 to the two diastereomers of 3-OH,2-$ONO_2$-CRALD and the two smaller peaks to the two diastereomers of 2-OH,3-$ONO_2$-CRALD. This assignment is corroborated by oxidation experiments using 3-hydroxybutanal (Technical grade, Chem Service Inc.), see Section S15. Experimen-

tal assignment of the two diasteromers of a given structural isomer of the crotonaldehyde hydroxy nitrates is not possible with the setup employed here in the absence of authentic diastereomerically pure standards. Instead, we assign these based on their calculated dipole moments which differ quite significantly between the different diastereomers (Table S15). GC elution order is not trivial to predict and depends on the boiling points of the analytes and the interaction between the analytes and the column. Considering molecules with similar size and functionality, species with higher dipole moments are likely to have stronger intermolecular interactions with themselves as well as stronger interactions with the polar trifluoropropyl groups of the column phase, both leading to longer retention times. Thus, we assume the diastereomer with the higher dipole moment elutes later from the column. For 2-OH,3-$ONO_2$ the *(R*,S*)*-diastereomer has the smallest dipole moment and is assumed to elute first, while the *(R*,R*)*-diastereomer is assumed to elute first for 3-OH,2-$ONO_2$. However, even if this assignment is incorrect, it will not affect the conclusions drawn regarding the stereoselectivity.

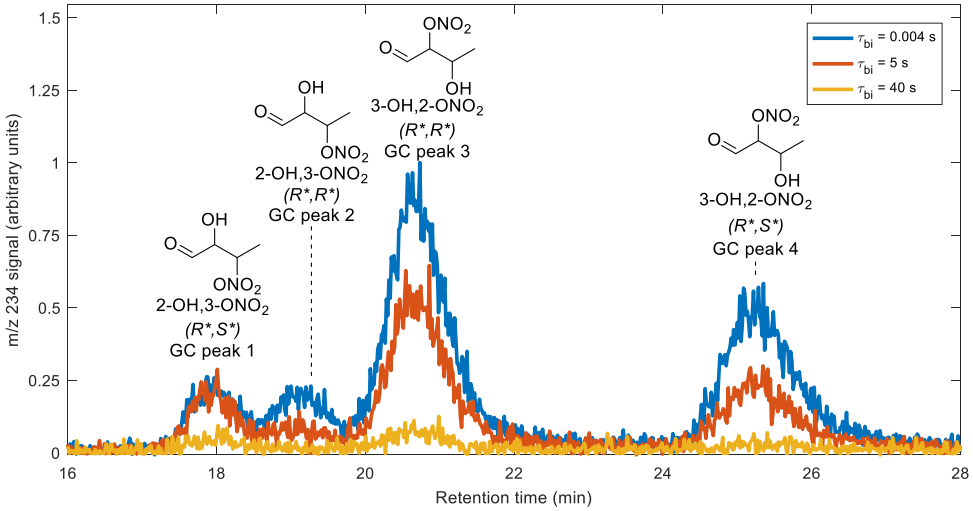


Figure 3: Chromatograms of the CRALD hydroxy nitrates (m/z 234) at different bimolecular lifetimes ($\tau_{bi}$). The signals have been scaled to the intensity of the second 2-methylpropene hydroxy nitrate peak (retention time = 8 min, not shown), which is added as a reference. T = 296 K.

The relative importance of the two OH-addition pathways in crotonaldehyde is assessed from the high-NO experiments (blue trace in Figure 3) and the calculated CIMS sensitivities of the formed hydroxy nitrates, assuming each has the same nitrate yield. As observed for the two smaller peaks eluting first, we expect the two diastereomers to be formed in similar amounts, as they are formed by $O_2$-addition to a near-planar alkyl radical.[31] The fact that the signal of the last-eluting crotonaldehyde hydroxy nitrate is almost a factor of two smaller than the other major hydroxy nitrate (when including estimated CIMS sensitivity, see Table S15) may be explained by a lower nitrate yield of the corresponding peroxy radical, a lower decomposition temperature or uncertainty in the calculated CIMS sensitivities. However, none of these affect the determined reaction rate coefficients, as their impact will be the same in all experiments. We estimate the branching between the two addition pathways to be about 10:90 favoring addition at the 3-position (see Section S19). This assumes that the abundance related to the fourth peak is equal to that of the third and that the nitrate yield is the same for all four peroxy radicals. Based on our experimental data, we estimate the overall nitrate yield for the reaction of crotonaldehyde hydroxy peroxy radicals with NO to be about 1.8 % (see Section S16). Further discussions of the mechanism and products of uni- and bimolecular chemistry of crotonaldehyde are given in Sections S20 and S21. The hydroxy nitrates produced from 2-methylpropene (m/z 220, Figure S13), which is added as a reference, are used to scale the crotonaldehyde HN signals. Specifically, 1-hydroxy-2-methylpropan-2-yl nitrate (the latter-eluting of its two HN peaks)[50] serves as the reference signal to normalize the CRALD peak areas to account for differences in OH and NO reactivity between experiments.

A clear decrease is observed in the normalized crotonaldehyde hydroxy nitrate yields (Figure 3) with increasing bimolecular lifetime ($\tau_{bimolecular}$). This is a clear indication of unimolecular chemistry of the crotonaldehyde hydroxy peroxy radicals. We calculate (Section S3.2) that for all isomers, the aldehydic H-shift is favored by at least a factor of 10 compared to the other potential H-shifts suggesting that this is the only important unimolecular pathway. At

a bimolecular lifetime of 40 s (Yellow trace in Figure 3), typical of atmospheric conditions in pristine environments, almost no crotonaldehyde hydroxy nitrates are formed. The observed rate of decrease in yield with increasing bimolecular lifetime is not the same for all four peaks indicating varying rate coefficients of the unimolecular H-shift reactions of the different isomers. Specifically, the *(R*,S*)* isomer of 2-OH,3-$ONO_2$-CRALD (GC peak 1, Figure 3), decreases markedly slower than the three remaining isomers. This suggests that the aldehydic H-shift in *(R*,S*)*-2-OH,3-OO-CRALD is slower than those in the other 3 isomers.

In Figure 4, we show the normalized (to the HN peak of the reference compound) crotonaldehyde hydroxy nitrate yields as a function of bimolecular lifetime (see Table S17). To facilitate comparison, the normalized HN yield for each isomer has been scaled to the average normalized HN yield in the short bimolecular lifetime experiments (highest NO). For all four hydroxy nitrate isomers, a distinct decrease in peak area ratio is observed as the bimolecular lifetime increases, reflecting the increased competition from the unimolecular reactions (Figure 2). For each isomer, the inflection point represents the bimolecular lifetime where the bimolecular and unimolecular chemistry are equally fast. The inverse of this value represents the rate coefficient of the unimolecular aldehydic H-shift at the temperature of the experiment.

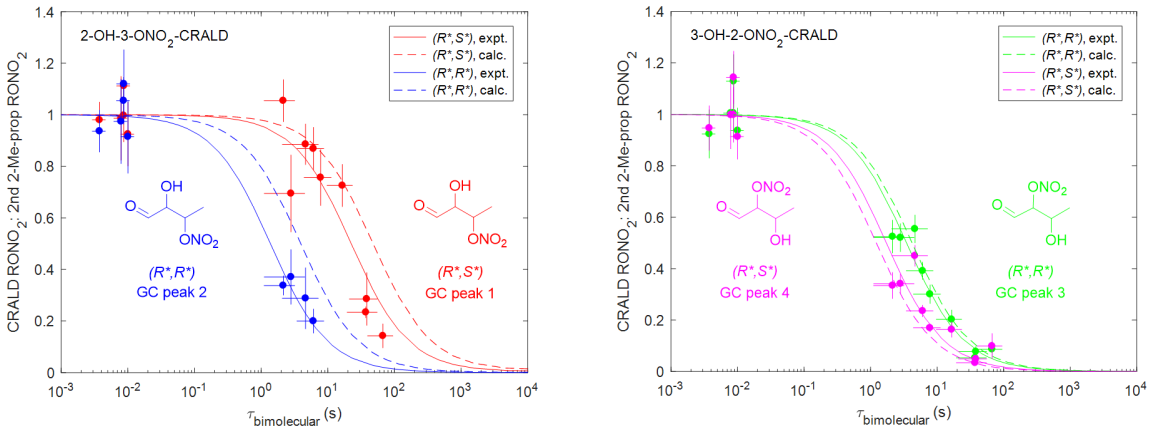


Figure 4: Normalized crotonaldehyde hydroxy nitrate yields scaled to the average short-bimolecular lifetime values as a function of the bimolecular lifetime ($\tau_{bimolecular}$). The solid lines represent the best model fit to the experimental data, while the dashed lines are the output from the chemical model using our calculated H-shift rate coefficients. T = 296 K.

The two diastereomers of 2-OH,3-OO-CRALD have markedly different H-shift rate coefficients (Figure 4, left panel). The yield of the *(R*,R*)* isomer decreases at a significantly shorter bimolecular lifetime compared to the *(R*,S*)* isomer indicating faster unimolecular chemistry. On the other hand, the rate coefficients for the two stereoisomers of 3-OH,2-OO-CRALD differ by a much smaller amount. The dashed lines in Figure 4 are from a model that incorporates the MC-TST calculated rate coefficients of the aldehydic H-shifts (Section S13).

Based on the best fit to the experimental data in Figure 4, we determine the rate coefficient for the aldehydic H-shift of each of the four isomers. These are given in Table 1 along with the corresponding calculated rate coefficient for the aldehydic H-shifts. We find that the difference in the experimental rate coefficients for the aldehydic H-shift is close to a factor of 20 between the two diastereomers of 2-OH,3-OO-CRALD. For the other structural isomer, the difference between the two diastereomers is only about a factor of two and within the estimated experimental uncertainty.

Table 1: Calculated and experimental reaction rate coefficients ($k_{calc}$ and $k_{expt}$, respectively, in $s^{-1}$) at 296 K.

| GC Peak nr. | Isomer | H-shift | $k_{calc}$[a] | $k_{expt}$[b] |
|---|---|---|---|---|
| 1 | *(R*,S*)*-2-OH,3-OO-CRALD[c] | 1,5 | 0.021 | 0.04 +0.03/-0.02 |
| 2 | *(R*,R*)*-2-OH,3-OO-CRALD[d] | 1,5 | 0.25 | 0.7 +1/-0.3 |
| 3 | *(R*,R*)*-3-OH,2-OO-CRALD[d] | 1,4 | 0.24 | 0.3 +0.2/-0.1 |
| 4 | *(R*,S*)*-3-OH,2-OO-CRALD[c] | 1,4 | 0.82 | 0.6 +0.4/-0.2 |

[a] Uncertainty in the calculated reaction rate coefficients is estimated to be about a factor of 10,[40] but agreement with available experimental values is better than a factor of 5.[30]
[b] The experimental uncertainty is determined based on the approach outlined in literature,[40,41] see Section S14.
[c] This includes *(R,S)* and *(S,R)*.
[d] This includes *(R,R)* and *(S,S)*.

For all four reactions, the experimentally determined reaction rate coefficients are in agreement with the calculated values to within a factor of three. Furthermore, the calculations correctly predicted a large stereo effect for 2-OH,3-OO-CRALD and a minor stereo effect for the 3-OH,2-OO-CRALD peroxy radical. In both cases, the calculations correctly determine which of the two diastereomers reacts the fastest (assuming the experimental diastereomer assignment is correct). The good performance of the theoretical approach by Møller et al.[36] for these reactions corroborates its performance for the other systems for which it has been employed.[36,40–42] This highlights the value and predictive power of high-level calculations, which can be performed for systems where experiments are not possible.

Previously, the calculated difference between diastereomers in 2-hexanol oxidation was suggested to be caused by differences in the hydrogen bonds available to the two diastereomers.[40] However, the reason for the differences observed here between the diastereomers of 2-OH,3-OO-CRALD is not obvious from their calculated lowest-conformer structures (Figure S4). Comparison of their zero-point corrected energies show that the reactant of *(R*,S*)*-2-OH,3-OO-CRALD is slightly lower in energy, while the TS is slightly higher in energy. This leads to a difference in the barrier height of 2.5 kcal/mol, producing the large difference in the cal-

culated rate coefficients. With subtle differences in barrier height having such large effects, the stereoselectivity is difficult to predict, which, in general, suggests that both stereoisomers need to be studied. The already challenging task of deriving structure-activity relationships (SARs) for peroxy radical H-shifts is thus further complicated.

The relatively large rate coefficients for aldehydic H-shift reactions found here are in good agreement with earlier experimental and theoretical studies.[30,36,49,51,52] Recent MC-TST calculated rate coefficients of a large number of peroxy radical H-shifts in the oxidation of isoprene found rate coefficients of 1,4; 1,5 and 1,6 aldehydic H-shifts in the range $6 \times 10^{-3}$ to $3 \times 10^{1}$ $s^{-1}$.[30] We have also calculated MC-TST rate coefficients for the aldehydic H-shifts in the hydroxy peroxy radicals formed from the crotonaldehyde-comparable compounds methacrolein and acrolein (Section S4) and find rate coefficients similar to those in Table 1. All available evidence suggests that aldehydic H-shifts are fast enough to outcompete bimolecular reactions under pristine conditions typical for regions of large VOC emissions and even be competitive in urban environments, especially in the future due to decreasing $NO_x$ emissions and increasing global average temperatures.[22,32,40,53]

A recent study reported weekend afternoon NO mixing ratios below 500 ppt in the L.A. basin corresponding to bimolecular peroxy radical lifetimes of more than 10 s.[40] At a bimolecular peroxy radical lifetime of 10 s, about 90 % of the *(R*,R*)*-2-OH,3-OO-CRALD isomer will react by the H-shift, while only about 35 % of the *(R*,S*)*-isomer will react by that pathway. This will lead to a large diastereomeric enhancement in the pools of products from the competing uni- and bimolecular chemistry: The *(R*,R*)*-diastereomer will be enhanced in unimolecular reaction products, while the *(R*,S*)*-diastereomer will be enhanced in the bimolecular reaction products. To the extent that such diastereomeric enhancements occur across the diverse set of substrates that comprise the VOC emitted to the atmosphere, they will influence the subsequent reactions in the atmosphere and the formation and properties

of atmospheric secondary organic aerosols.[19,22] This highlights the importance of considering the stereochemistry in the context of atmospheric oxidation and H-shifts, especially as even larger stereo effects have been calculated recently for more complex systems formed in the oxidation of isoprene with more complicated hydrogen bonding patterns available.[30] Atmospheric enhancement of specific stereoisomers by stereoselective gas-phase reactions could have widespread implications given the ubiquity of chirality in nature.

# Methods

*Experimental.* Experiments are performed in a ~1 $m^3$ Teflon chamber at ambient atmospheric pressure (~745 Torr) and temperature (296 K). A standard mixture of crotonaldehyde and 2-methylpropene (serving as an external reference for the rate of bimolecular chemistry) and oxidation was initiated by photolysis of methyl nitrite producing OH. Products are measured using chemical ionization time-of-flight mass spectrometry (CI-ToF-MS, Tofwerk, Caltech) using $CF_3O^-$ as reagent ion, as described in detail before.[54,55] The stereoisomeric compounds are separated using an 11.5 m Restek RTX-200 megabore GC column (I.D. = 0.53 mm, $d_f$ = 3.00 $\mu$m) gas chromatography column placed in a Varian CP-3800 gas chromatograph (GC) oven. Experiments are conducted with different concentrations of $HO_2$ and NO to vary the bimolecular lifetime of the peroxy radical. The bimolecular lifetime is determined as described previously.[40,41,56] The H-shift rate coefficients are extracted by fitting a simple chemical model (Section S13) to the crontonaldehyde HN yield (normalized to the second peak of 2-methylpropene HN) as a function of the determined bimolecular lifetime. The experimental procedure is described in detail in Section S9.

*Computational.* Reaction rate coefficients are calculated using the approach by Møller et al.[36] This approach uses multi-conformer transition state theory (MC-TST),[36,43] with barrier heights calculated at the ROHF-RCCSD(T)-F12a/cc-pVDZ-F12//$\omega$B97X-D/aug-cc-pVTZ

level in Molpro 2012.1.[57–65] Partition functions and relative energies between conformers calculated using ωB97X-D/aug-cc-pVTZ in Gaussian 09, revision D.01.[57–59,66] Tunneling coefficients are calculated using the Eckart approach.[67] Details on the computational approach are given in Section S1.

# Supporting Information Available

Theoretical methods, assessment of the conformational sampling approach, calculated H-shift rate coefficients and associated data, temperature dependence of the calculated aldehydic H-shift rate coefficients, calculated alkyl radical stabilities, comparison of alkoxy bond scissions, CIMS sensitivities, experimental methods, initial experimental mixing ratios, approach for determination of bimolecular lifetime, evaluation of the importance of $RO_2 + RO_2$ chemistry, simple chemical model to obtain experimental H-shift rate coefficients, uncertainty in the experimental reaction rate coefficients, 3-hydroxybutanal oxidation, discussion of hydroxy nitrate yields, chromatograms, $NO_3$ experiment results, high-NO oxidation mechanism, growth of possible products from NO chemistry, oxidation mechanism following aldehydic H-shifts and crotonaldehyde peak area ratios.

All ωB97X-D/aug-cc-pVTZ and F12 output files, which include the ωB97X-D/aug-cc-pVTZ optimized geometries, are available at:

https://sid.erda.dk/public/archives/bfad8e9ca7cf171e6d225371b36c3372/published-archive.html

# Author Information

## Corresponding Author

* (P.O.W.): E-mail: wennberg@caltech.edu

* (H.G.K.): E-mail: hgk@chem.ku.dk

## ORCID

Kristian H. Møller: 0000-0001-8070-8516

Eric Praske: 0000-0001-7169-4423

Lu Xu: 0000-0002-0021-9876

John D. Crounse: 0000-0001-5443-729X

Paul O. Wennberg: 0000-0002-6126-3854

Henrik G. Kjaergaard: 0000-0002-7275-8297


## Notes

The authors declare no competing financial interest.

# Acknowledgement

The authors thank Hannah M. Allen for helpful discussions. K. H. M. acknowledges the financial support of the Danish Ministry for Higher Education and Science's Elite Research travel grant and the Niels Bohr Foundation. We are grateful for the funding from the National Science Foundation (Grant CHE-1508526), the Alfred P. Sloan Foundation's program Chemistry of Indoor Environments, the Independent Research Fund Denmark and the University of Copenhagen.

# References

(1) Meierhenrich, U. *Amino Acids and the Asymmetry of Life*, 1st ed.; Springer-Verlag Berlin Heidelberg, 2008.

(2) Blackmond, D. G. The Origin of Biological Homochirality. *Philos. Trans. R. Soc. B: Bio. Sci.* **2011**, *366*, 2878–2884.

(3) McGuire, B. A.; Carroll, P. B.; Loomis, R. A.; Finneran, I. A.; Jewell, P. R.; Remijan, A. J.; Blake, G. A. Discovery of the Interstellar Chiral Molecule Propylene Oxide ($CH_3CHCH_2O$). *Science* **2016**, *352*, 1449–1452.

(4) Kesselmeier, J.; Staudt, M. Biogenic Volatile Organic Compounds (VOC): An Overview on Emission, Physiology and Ecology. *J. Atmos. Chem.* **1999**, *33*, 23–88.

(5) Guenther, A. B.; Jiang, X.; Heald, C. L.; Sakulyanontvittaya, T.; Duhl, T.; Emmons, L. K.; Wang, X. The Model of Emissions of Gases and Aerosols from Nature version 2.1 (MEGAN2.1): An Extended and Updated Framework for Modeling Biogenic Emissions. *Geosci. Model Dev.* **2012**, *5*, 1471–1492.

(6) Williams, J.; Yassaa, N.; Bartenbach, S.; Lelieveld, J. Mirror Image Hydrocarbons from Tropical and Boreal Forests. *Atmos. Chem. Phys.* **2007**, *7*, 973–980.

(7) Yassaa, N.; Brancaleoni, E.; Frattoni, M.; Ciccioli, P. Trace Level Determination of Enantiomeric Monoterpenes in Terrestrial Plant Emission and in the Atmosphere using a $\beta$-Cyclodextrin Capillary Column Coupled with Thermal Desorption and Mass Spectrometry. *J. Chromatogr. A* **2001**, *915*, 185 – 197.

(8) Song, W.; Williams, J.; Yassaa, N.; Martinez, M.; Carnero, J. A. A.; Hidalgo, P. J.; Bozem, H.; Lelieveld, J. Winter and Summer Characterization of Biogenic Enantiomeric Monoterpenes and Anthropogenic BTEX Compounds at a Mediterranean Stone Pine Forest Site. *J. Atmos. Chem.* **2011**, *68*, 233–250.

(9) Yassaa, N.; Williams, J. Enantiomeric Monoterpene Emissions from Natural and Damaged Scots Pine in a Boreal Coniferous Forest Measured using Solid-Phase Microextraction and Gas Chromatography/Mass Spectrometry. *J. Chromatogr. A* **2007**, *1141*, 138 – 144.

(10) Yassaa, N.; Song, W.; Lelieveld, J.; Vanhatalo, A.; Bäck, J.; Williams, J. Diel Cycles of Isoprenoids in the Emissions of Norway Spruce, Four Scots Pine Chemotypes, and in

Boreal Forest Ambient Air during HUMPPA-COPEC-2010. *Atmos. Chem. Phys.* **2012**, *12*, 7215–7229.

(11) Salma, I.; Mészáros, T.; Maenhaut, W.; Vass, E.; Majer, Z. Chirality and the Origin of Atmospheric Humic-Like Substances. *Atmos. Chem. Phys.* **2010**, *10*, 1315–1327.

(12) Ebben, C. J.; Zorn, S. R.; Lee, S.-B.; Artaxo, P.; Martin, S. T.; Geiger, F. M. Stereochemical Transfer to Atmospheric Aerosol Particles Accompanying the Oxidation of Biogenic Volatile Organic Compounds. *Geophys. Res. Lett.* **2011**, *38*, L16807.

(13) Nozière, B.; González, N. J.; Borg-Karlson, A.-K.; Pei, Y.; Redeby, J. P.; Krejci, R.; Dommen, J.; Prevot, A. S. H.; Anthonsen, T. Atmospheric Chemistry in Stereo: A New Look at Secondary Organic Aerosols from Isoprene. *Geophys. Res. Lett.* **2011**, *38*, L11807.

(14) Martinez, I. S.; Peterson, M. D.; Ebben, C. J.; Hayes, P. L.; Artaxo, P.; Martin, S. T.; Geiger, F. M. On Molecular Chirality within Naturally Occurring Secondary Organic Aerosol Particles from the Central Amazon Basin. *Phys. Chem. Chem. Phys.* **2011**, *13*, 12114–12122.

(15) Katsumoto, Y.; Kubosaki, N.; Miyata, T. Molecular Approach To Understand the Tacticity Effects on the Hydrophilicity of Poly(*N*-isopropylacrylamide): Solubility of Dimer Model Compounds in Water. *J. Phys. Chem. B* **2010**, *114*, 13312–13318.

(16) Chang, L.; Woo, E. M. Tacticity Effects on Glass Transition and Phase Behavior in Binary Blends of Poly(Methyl Methacrylate)s of Three Different Configurations. *Polym. Chem.* **2010**, *1*, 198–202.

(17) Tachibana, T.; Yoshizumi, T.; Hori, K. Monolayer Studies of Chiral and Racemic 12-Hydroxyoctadecanoic Acids. *Bull. Chem. Soc. Jpn.* **1979**, *52*, 34–41.

(18) Fuhrhop, J. H.; Schnieder, P.; Rosenberg, J.; Boekema, E. The Chiral Bilayer Effect Stabilizes Micellar Fibers. *J. Am. Chem. Soc.* **1987**, *109*, 3387–3390.

(19) Cash, J. M.; Heal, M. R.; Langford, B.; Drewer, J. A Review of Stereochemical Implications in the Generation of Secondary Organic Aerosol from Isoprene Oxidation. *Environ. Sci.: Process. Impacts* **2016**, *18*, 1369–1380.

(20) Mikhailov, E.; Vlasenko, S.; Martin, S. T.; Koop, T.; Pöschl, U. Amorphous and Crystalline Aerosol Particles Interacting with Water Vapor: Conceptual Framework and Experimental Evidence for Restructuring, Phase Transitions and Kinetic Limitations. *Atmos. Chem. Phys.* **2009**, *9*, 9491–9522.

(21) Freney, E. J.; Adachi, K.; Buseck, P. R. Internally Mixed Atmospheric Aerosol Particles: Hygroscopic Growth and Light Scattering. *J. Geophys. Res. Atmos.* **2010**, *115*, D19210.

(22) Boucher, O.; Randall, D.; Artaxo, P.; Bretherton, C.; Feingold, G.; Forster, P.; Kerminen, V.-M.; Kondo, Y.; Liao, H.; Lohmann, U. et al. In *Climate Change 2013: The Physical Science Basis. Contribution of Working Group I to the Fifth Assessment Report of the Intergovernmental Panel on Climate Change*; Stocker, T., Qin, D., Plattner, G.-K., Tignor, M., Allen, S., Boschung, J., Nauels, A., Xia, Y., Bex, V., Midgley, P., Eds.; Cambridge University Press: Cambridge, United Kingdom and New York, NY, USA, 2013; Chapter 7, p 571–658.

(23) Stokes, G. Y.; Chen, E. H.; Buchbinder, A. M.; Paxton, W. F.; Keeley, A.; Geiger, F. M. Atmospheric Heterogeneous Stereochemistry. *J. Am. Chem. Soc.* **2009**, *131*, 13733–13737.

(24) Crounse, J. D.; Nielsen, L. B.; Jørgensen, S.; Kjaergaard, H. G.; Wennberg, P. O. Autoxidation of Organic Compounds in the Atmosphere. *J. Phys. Chem. Lett.* **2013**, *4*, 3513–3520.

(25) Ehn, M.; Thornton, J.; Kleist, E.; Sipilä, M.; Junninen, H.; Pullinen, I.; Springer, M.; Rubach, F.; Tillmann, R.; Lee, B. et al. A Large Source of Low-Volatility Secondary Organic Aerosol. *Nature* **2014**, *506*, 476–479.

(26) Kroll, J. H.; Seinfeld, J. H. Chemistry of Secondary Organic Aerosol: Formation and Evolution of Low-Volatility Organics in the Atmosphere. *Atmos. Environ.* **2008**, *42*, 3593 – 3624.

(27) Slowik, J. G.; Stroud, C.; Bottenheim, J. W.; Brickell, P. C.; Chang, R. Y.-W.; Liggio, J.; Makar, P. A.; Martin, R. V.; Moran, M. D.; Shantz, N. C. et al. Characterization of a Large Biogenic Secondary Organic Aerosol Event from Eastern Canadian Forests. *Atmos. Chem. Phys.* **2010**, *10*, 2825–2845.

(28) Bianchi, F.; Kurtén, T.; Riva, M.; Mohr, C.; Rissanen, M. P.; Roldin, P.; Berndt, T.; Crounse, J. D.; Wennberg, P. O.; Mentel, T. F. et al. Highly Oxygenated Organic Molecules (HOM) from Gas-Phase Autoxidation Involving Peroxy Radicals: A Key Contributor to Atmospheric Aerosol. *Chem. Rev.* **2019**, *119*, 3472–3509.

(29) Barsanti, K. C.; Kroll, J. H.; Thornton, J. A. Formation of Low-Volatility Organic Compounds in the Atmosphere: Recent Advancements and Insights. *J. Phys. Chem. Lett.* **2017**, *8*, 1503–1511.

(30) Møller, K. H.; Bates, K. H.; Kjaergaard, H. G. The Importance of Peroxy Radical Hydrogen-Shift Reactions in Atmospheric Isoprene Oxidation. *J. Phys. Chem. A* **2019**, *123*, 920–932.

(31) Symons, M. C. R. Shape of Alkyl Radicals by Electron Spin Resonance. *Nature* **1969**, *222*, 1123–1124.

(32) Orlando, J. J.; Tyndall, G. S. Laboratory Studies of Organic Peroxy Radical Chemistry: An Overview with Emphasis on Recent Issues of Atmospheric Significance. *Chem. Soc. Rev.* **2012**, *41*, 6294–6317.

(33) Poppe, L.; Nagy, J.; Hornyánszky, G.; Boros, Z. In *Stereochemistry and Stereoselective Synthesis: An Introduction*; Nógrádim, M., Poppe, L., Eds.; Wiley-VCH Verlag GmbH & Co. KGaA, 2016.

(34) Jenkin, M. E.; Valorso, R.; Aumont, B.; Rickard, A. R. Estimation of Rate Coefficients and Branching Ratios for Reactions of Organic Peroxy Radicals for use in Automated Mechanism Construction. *Atmos. Chem. Phys.* **2019**, *19*, 7691–7717.

(35) Bates, K. H.; Jacob, D. J. A New Model Mechanism for Atmospheric Oxidation of Isoprene: Global Effects on Oxidants, Nitrogen Oxides, Organic Products, and Secondary Organic Aerosol. *Atmos. Chem. Phys.* **2019**, *19*, 9613–9640.

(36) Møller, K. H.; Otkjær, R. V.; Hyttinen, N.; Kurtén, T.; Kjaergaard, H. G. Cost-Effective Implementation of Multiconformer Transition State Theory for Peroxy Radical Hydrogen Shift Reactions. *J. Phys. Chem. A* **2016**, *120*, 10072–10087.

(37) Mohamed, S. Y.; Davis, A. C.; Al Rashidi, M. J.; Sarathy, S. M. High-Pressure Limit Rate Rules for $\alpha$-H Isomerization of Hydroperoxyalkylperoxy Radicals. *J. Phys. Chem. A* **2018**, *122*, 3626–3639.

(38) Mohamed, S. Y.; Davis, A. C.; Al Rashidi, M. J.; Sarathy, S. M. Computational Kinetics of Hydroperoxybutylperoxy Isomerizations and Decompositions: A Study of the Effect of Hydrogen Bonding. *J. Phys. Chem. A* **2018**, *122*, 6277–6291.

(39) Otkjær, R. V.; Jakobsen, H. H.; Tram, C. M.; Kjaergaard, H. G. Calculated Hydrogen Shift Rate Constants in Substituted Alkyl Peroxy Radicals. *J. Phys. Chem. A* **2018**, *122*, 8665–8673.

(40) Praske, E.; Otkjær, R. V.; Crounse, J. D.; Hethcox, J. C.; Stoltz, B. M.; Kjaergaard, H. G.; Wennberg, P. O. Atmospheric Autoxidation is Increasingly Important in Urban and Suburban North America. *Proc. Natl. Acad. Sci. U.S.A.* **2018**, *115*, 64–69.

(41) Praske, E.; Otkjær, R. V.; Crounse, J. D.; Hethcox, J. C.; Stoltz, B. M.; Kjaergaard, H. G.; Wennberg, P. O. Intramolecular Hydrogen Shift Chemistry of Hydroperoxy-Substituted Peroxy Radicals. *J. Phys. Chem. A* **2019**, *123*, 590–600.

(42) Xu, L.; Møller, K. H.; Crounse, J. D.; Otkjær, R. V.; Kjaergaard, H. G.; Wennberg, P. O. Unimolecular Reactions of Peroxy Radicals Formed in the Oxidation of $\alpha$-Pinene and $\beta$-Pinene by Hydroxyl Radicals. *J. Phys. Chem. A* **2019**, *123*, 1661–1674.

(43) Vereecken, L.; Peeters, J. The 1,5-H-shift in 1-Butoxy: A Case Study in the Rigorous Implementation of Transition State Theory for a Multirotamer System. *J. Chem. Phys.* **2003**, *119*, 5159–5170.

(44) Kerr, J. A.; Sheppard, D. W. Kinetics of the Reactions of Hydroxyl Radicals with Aldehydes Studied under Atmospheric Conditions. *Environ. Sci. Technol.* **1981**, *15*, 960–963.

(45) Atkinson, R.; Aschmann, S. M.; Pitts, J. N. Kinetics of the Gas-Phase Reactions of OH Radicals with a Series of $\alpha$,$\beta$-Unsaturated Carbonyls at 299 $\pm$ 2 K. *Int. J. Chem. Kinet.* **1983**, *15*, 75–81.

(46) Magneron, I.; Thévenet, R.; Mellouki, A.; Le Bras, G.; Moortgat, G. K.; Wirtz, K. A Study of the Photolysis and OH-initiated Oxidation of Acrolein and *trans*-Crotonaldehyde. *J. Phys. Chem. A* **2002**, *106*, 2526–2537.

(47) Orlando, J. J.; Tyndall, G. S. Mechanisms for the Reactions of OH with Two Unsaturated Aldehydes: Crotonaldehyde and Acrolein. *J. Phys. Chem. A* **2002**, *106*, 12252–12259.

(48) Kwok, E. S.; Atkinson, R. Estimation of Hydroxyl Radical Reaction Rate Constants for Gas-Phase Organic Compounds using a Structure-Reactivity Relationship: An Update. *Atmos. Environ.* **1995**, *29*, 1685 – 1695.

(49) Crounse, J. D.; Knap, H. C.; Ørnsø, K. B.; Jørgensen, S.; Paulot, F.; Kjaergaard, H. G.; Wennberg, P. O. Atmospheric Fate of Methacrolein. 1. Peroxy Radical Isomerization Following Addition of OH and $O_2$. *J. Phys. Chem. A* **2012**, *116*, 5756–5762.

(50) Teng, A. P.; Crounse, J. D.; Lee, L.; St. Clair, J. M.; Cohen, R. C.; Wennberg, P. O. Hydroxy Nitrate Production in the OH-Initiated Oxidation of Alkenes. *Atmos. Chem. Phys.* **2015**, *15*, 4297–4316.

(51) Rissanen, M. P.; Kurtén, T.; Sipilä, M.; Thornton, J. A.; Kangasluoma, J.; Sarnela, N.; Junninen, H.; Jørgensen, S.; Schallhart, S.; Kajos, M. K. et al. The Formation of Highly Oxidized Multifunctional Products in the Ozonolysis of Cyclohexene. *J. Am. Chem. Soc.* **2014**, *136*, 15596–15606.

(52) Knap, H. C.; Jørgensen, S. Rapid Hydrogen Shift Reactions in Acyl Peroxy Radicals. *J. Phys. Chem. A* **2017**, *121*, 1470–1479.

(53) Hidy, G. M.; Blanchard, C. L.; Baumann, K.; Edgerton, E.; Tanenbaum, S.; Shaw, S.; Knipping, E.; Tombach, I.; Jansen, J.; Walters, J. Chemical Climatology of the Southeastern United States, 1999-2013. *Atmos. Chem. Phys.* **2014**, *14*, 11893–11914.

(54) Crounse, J. D.; McKinney, K. A.; Kwan, A. J.; Wennberg, P. O. Measurement of Gas-Phase Hydroperoxides by Chemical Ionization Mass Spectrometry. *Anal. Chem.* **2006**, *78*, 6726–6732.

(55) Vasquez, K. T.; Allen, H. M.; Crounse, J. D.; Praske, E.; Xu, L.; Noelscher, A. C.; Wennberg, P. O. Low-Pressure Gas Chromatography with Chemical Ionization Mass Spectrometry for Quantification of Multifunctional Organic Compounds in the Atmosphere. *Atmospheric Meas. Tech.* **2018**, *11*, 6815–6832.

(56) Crounse, J. D.; Paulot, F.; Kjaergaard, H. G.; Wennberg, P. O. Peroxy Radical Isomerization in the Oxidation of Isoprene. *Phys. Chem. Chem. Phys.* **2011**, *13*, 13607–13613.

(57) Chai, J.-D.; Head-Gordon, M. Long-range Corrected Hybrid Density Functionals with Damped Atom-atom Dispersion Corrections. *Phys. Chem. Chem. Phys.* **2008**, *10*, 6615–6620.

(58) Dunning, T. H. Gaussian Basis Sets for Use in Correlated Molecular Calculations. I. The Atoms Boron Through Neon and Hydrogen. *J. Chem. Phys.* **1989**, *90*, 1007–1023.

(59) Kendall, R. A.; Dunning, T. H.; Harrison, R. J. Electron Affinities of the First-row Atoms Revisited. Systematic Basis Sets and Wave Functions. *J. Chem. Phys.* **1992**, *96*, 6796–6806.

(60) Werner, H.-J.; Knowles, P. J.; Knizia, G.; Manby, F. R.; Schütz, M.; Celani, P.; Györffy, W.; Kats, D.; Korona, T.; Lindh, R. et al. MOLPRO, Version 2012.1, a Package of Ab Initio Programs. 2012; see http://www.molpro.net.

(61) Watts, J. D.; Gauss, J.; Bartlett, R. J. Coupled-cluster Methods with Noniterative Triple Excitations for Restricted Open-shell Hartree-Fock and Other General Single Determinant Reference Functions. Energies and Analytical Gradients. *J. Chem. Phys.* **1993**, *98*, 8718–8733.

(62) Adler, T. B.; Knizia, G.; Werner, H.-J. A Simple and Efficient CCSD(T)-F12 Approximation. *J. Chem. Phys.* **2007**, *127*, 221106.

(63) Knizia, G.; Adler, T. B.; Werner, H.-J. Simplified CCSD(T)-F12 Methods: Theory and Benchmarks. *J. Chem. Phys.* **2009**, *130*, 054104.

(64) Werner, H.-J.; Knizia, G.; Manby, F. R. Explicitly Correlated Coupled Cluster Methods with Pair-Specific Geminals. *Mol. Phys.* **2011**, *109*, 407–417.

(65) Peterson, K. A.; Adler, T. B.; Werner, H.-J. Systematically Convergent Basis Sets for Explicitly Correlated Wavefunctions: The Atoms H, He, B–Ne, and Al–Ar. *J. Chem. Phys.* **2008**, *128*, 084102.

(66) Frisch, M. J.; Trucks, G. W.; Schlegel, H. B.; Scuseria, G. E.; Robb, M. A.; Cheeseman, J. R.; Scalmani, G.; Barone, V.; Mennucci, B.; Petersson, G. A. et al. Gaussian 09 Revision D.01. Gaussian Inc. Wallingford CT 2009.

(67) Eckart, C. The Penetration of a Potential Barrier by Electrons. *Phys. Rev.* **1930**, *35*, 1303–1309.